Journal of Hydrology: Regional Studies 56 (2024) 102027

Contents lists available at ScienceDirect

Journal of Hydrology: Regional Studies

journal homepage: www.elsevier.com/locate/ejrh

Analysis of turbidity current plunging and floating woody debris in a reservoir during flood events

Fong-Zuo Lee [a], Jihn-Sung Lai [b,*], Sameh Ahmed Kantoush [c], Tetsuya Sumi [c]

[a] *Department of Civil Engineering, National Chung Hsing University, 145 Xingda Rd., South Dist, Taichung City 402202, Taiwan*

[b] *Hydrotech Research Institute and Department of Bioenvironmental Systems Engineering, National Taiwan University, No. 1, Section 4, Roosevelt Rd., Taipei City 106319, Taiwan*

[c] *Disaster Prevention Research Institute (DPRI), Kyoto University, Goka-sho, Uji-shi 611-0011, Japan*

A R T I C L E I N F O

Keywords:
Turbidity current
Woody debris
Plunge point
Densimetric Froude number
Inflow peak sediment yield

A B S T R A C T

Study region: Many reservoirs worldwide experience the challenge of managing woody debris and determining the feasible location to set a floating barrier as a mitigation strategy to restrict their progression towards the dam. While the turbidity current plunges along the reservoir bed to form the underflow mud layer, the reverse current generated in the plunging flow region holds the woody debris.

Study focus: The present study attempts to define the plunging zone in correlation with the floating woody debris based on field observations, densimetric Froude number, plunging formula, and entrainment formula to investigate the plunge point location. When woody debris is carried by the sediment-laden inflow through the reservoir, the volume of woody debris needs to be estimated and extracted after the flood recession.

New hydrological insight for the region: According to the results of the analysis, the plunge point location was suggested as the critical condition of the densimetric Froude number for a floating barrier setup. Two proposed equations are presented to identify the turbidity current vertical profiles of velocity and sediment concentration. Considering hydrological conditions, the inflow peak sediment yield has added an optimal quantitative estimation of woody debris volumes than that by inflow peak discharge, total inflow sediment yield, maximum rainfall intensity, and total rainfall. The presented threshold values of hydrological patterns can serve as a critical warning indicator for the preparation of extraction operations for floating woody debris.

1. Introduction

During a flood, a river naturally transports significant quantities of sediment from the upstream watershed, typically with vulnerable geological features. Due to the decrease in flow velocity in still and deep regions, i.e., reservoir, deposition of coarser sediment, which gets transported with water flow, occurs near the delta. Meanwhile, fine suspended sediments may create a turbidity current progressing toward the dam. Dominated by the presence of suspended sediments, the turbidity current moves into a relatively lighter ambient fluid in a reservoir, which may plunge and progress as an underflow along the reservoir bottom. If there is insufficient outlet discharge capacity to sluice the incoming turbidity current, the turbidity current may form a submerged muddy lake when it

* Corresponding author.
E-mail addresses: fzlee@nchu.edu.tw (F.-Z. Lee), jslai525@ntu.edu.tw (J.-S. Lai), kantoush.samehahmed.2n@kyoto-u.ac.jp (S.A. Kantoush), sumi.tetsuya.2s@kyoto-u.ac.jp (T. Sumi).

https://doi.org/10.1016/j.ejrh.2024.102027
Received 11 June 2024; Received in revised form 3 October 2024; Accepted 13 October 2024
Available online 10 November 2024
2214-5818/

arrives at the dam. Therefore, many researchers have investigated the phenomenon of turbidity current formation and movement in a reservoir to understand its impact on sedimentation inside the reservoir (Brasington and Richards, 2000; Minella et al., 2008; Wang et al., 2013; Schleiss et al., 2016; Ehmann et al., 2019; Chen, 2022; Hung et al., 2022; Panagos et al., 2024) and its influence on the downstream (Lee et al., 2022). In addition, sensitivity analysis is vital for the effective monitoring and management of natural resources as water, particularly amid climate change challenges. It enables the assessment of diverse scenarios, optimizing hydraulic engineering solutions and Nature Based Solutions (NBS) for flood risk management. By comparing various reservoir configurations, sensitivity analysis helps in swiftly evaluating reduction effects and refining designs (Lama et al., 2021; Pirone et al., 2024). In the Cantareira System, it supports soil conservation policies by identifying sediment sources and modeling soil losses, thus mitigating erosion and enhancing water reservoir sustainability. Ultimately, sensitivity analysis ensures informed decision-making, promoting the protection and sustainable use of ecosystems and water resources (Lense et al., 2023).

Flume experiments and field measurements have shown that the occurrence of turbidity plunging can be related to flow velocity, water depth, and differential fluid density. The phenomenon of plunging density flows has been studied by several researchers, including Singh and Shah (1971), Wunderlich and Elder (1973), Savage and Brimberg (1975), Hebbert et al. (1979), Jain (1981), Graf (1983), Akiyama and Stefan (1984), Farrel and Stefan (1988), Lee and Yu (1997), Bournet et al. (1999), Parker and Toniolo (2007), Dai and Garcia (2007), (2009a), (2009b), Chen (2017), Lee et al. (2019) and Chang et al. (2020). Those studies have focused on the theoretical conditions and assumptions of the plunging point location at which the adapted densimetric Frounde number ranges between 0.3 and 1.0 near the location where is the plunge point. Therefore, the present study focuses on the field observation data and compares the distinguished methods proposed by Parker et al. (1987), Parker and Toniolo (2007), and Lee et al. (2019) to investigate the plunging point location in a reservoir.

In a natural flow regime of a mountainous region, a flood event is generally followed by a flash flood transporting sediments as well

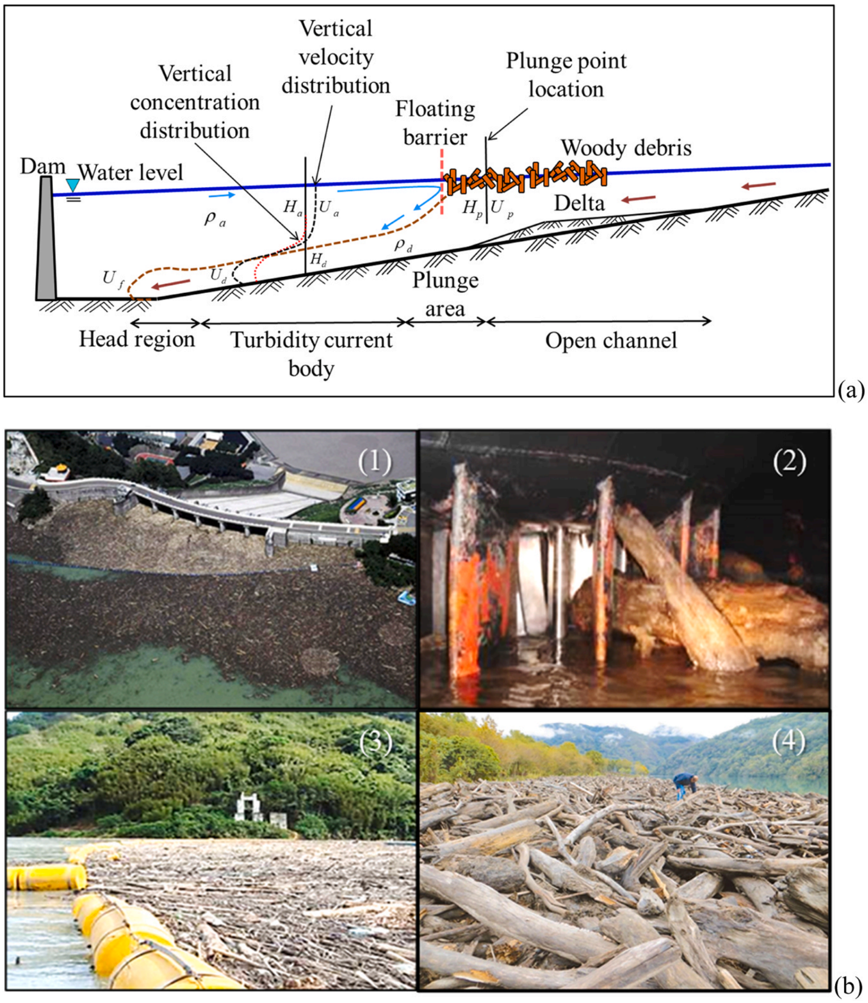

Fig. 1. Descriptions of turbidity current and floating woody debris: (a) illustration of turbidity current plunging region with velocity and concentration distributions; (b) (1) massive woody debris accumulation in front of the dam, (2) clogged in power generating turbine (modified from Water Resources Planning Branch, 2020), (3) the floating barrier with collected woody debris, (4) placement field of extracted woody debris.

as woody debris (Ruiz-Villanueva et al., 2013). When such sediment-laden flow with floating woody debris gets transported into a reservoir, the plunge location will act as a separation point for the sediment-laden flow and floating woody debris. At the plunge point, the mechanism of river flow with high sediment concentration plunging into the ambient water of a reservoir is illustrated in Fig. 1(a). The sketch presented in Fig. 1(a) shows the turbidity current plunges and forms a dense underflow along the inclined reservoir bottom. During a flood event, the sediment-laden flow enters and disappears at the upstream limit of a reservoir. This phenomenon frequently observed from the water surface indicates the plunging of a turbidity current. The plunge point location may be regarded as a sharp transition between turbid and clear water or by the accumulation of floating woody debris with zero velocity points. Suppose there are suitable conditions for measuring in the field during a flood. In that case, the turbidity current may be recognized by sediment concentration and velocity profiling equipment, which distinguishes the inflowing and impounded waters (Morris and Fan, 2010).

Numerical models and advanced solving mechanisms have been developed to simulate water-sediment interactions, focusing on phenomena such as turbidity currents, sediment flushing, deposition patterns, and sediment discharge through outlets (Busico et al., 2020; Hung, 2024; Imtiyaz et al., 2024; Lee and Huynh Nguyen, 2024). While these models provide valuable insights, each dimensional model has its own limitations and drawbacks. One key limitation is the lack of integration between sediment-laden flows and floating woody debris, a crucial factor in understanding sediment transport dynamics. Physical modeling, on the other hand, has been widely employed in hydraulic engineering to address design and operational challenges. It uses scaled models to replicate water and sediment transport processes in various natural flow systems (Ettema et al., 2000). Numerous advanced studies have leveraged physical modeling to explore sediment transport in reservoirs or to assess the effects of bottom roughness in streams (Crimaldi and Lama, 2021; Huang, et al., 2023). These physical models provide detailed visualizations and real-time data but face practical challenges. The size limitations of experimental sites, high labor demands, and economic constraints make it difficult to carry out large-scale studies. As a result, few studies have been conducted to examine sediment-laden flows that also include floating woody debris, despite their potential significance in sediment transport processes. Developing a more comprehensive model that incorporates both sediment and debris dynamics would be essential for advancing our understanding and improving reservoir management and sediment mitigation strategies.

After heavy rainfall in the watershed, the river flood carries high sediment concentration and floating debris in the streams. Woody debris produced from upstream watersheds entering rivers provides various habitat structures for aquatic ecosystems. However, during a flood, woody debris is subjected to flowing into a reservoir, and it may damage hydraulic structures such as spillway gates, block flow passage, or clog the hydropower turbine (Vaughn et al., 2021). During the flood period of Typhoon Aere in 2004, as an example, a great amount of floating woody debris had accumulated in front of the Shihmen dam, which blocked all the entrances of spillways and the gaps of the trash rack at the intakes, and damaged the power generating turbine (as shown in Fig. 1(b)(1) and 1(b)(2)). On the other hand, dredging sediment deposits from the reservoir bottom can be costly and challenging if the floating woody debris sinks and deposits. In the European Union (EU) and Switzerland, the costs for sediment removal range from 2 to 50€per m^3 (Panagos et al., 2024). Therefore, setting a floating barrier usually is employed as a mitigation strategy to restrict woody debris progression toward the dam. Meanwhile, when woody debris is carried by the sediment-laden inflow through the reservoir, the volume of woody debris needs to be estimated and extracted after the flood recession. Only a few researchers have investigated the extracted volume of woody debris in the reservoir during flood events. By surveying woody debris quantity on the upper Rhone River (France), Moulin and Piegay (2004) estimated woody debris volume extracted from the Genissiat dam's reservoir by using a linear regression formula related to the peak flow discharge. Seo et al. (2012) examined the relationships between large wood (LW) export and precipitation patterns and intensity by analyzing the data on the annual volume of LW removed from 42 reservoirs and the daily precipitation at or near the reservoir sites.

Furthermore, Fig. 1(a) also illustrates the flow phenomenon of turbidity current and woody debris trapped by flow circulation near the plunge point location and dam site. Before turbidity current generation, woody debris flowed into the reservoir and spread everywhere. When turbidity current developed, due to continuity assumption, turbidity current flow near the bottom would induce an upper circulation to trap woody debris, and the trap location is close to the plunge point location. Then, when the woody debris becomes denser than the turbidity current due to sediment cladding and water uptake effects, some woody debris may flow with the turbidity current and migrate near the bottom. The field survey showed that when woody debris flowed with the turbidity current into hydraulic works, such as power plants, the structures were damaged and clogged with woody debris. Therefore, avoiding the woody debris flowing into the intake was an essential concept of intake operation. Usually, there are two methods are executed to prevent woody debris from washing into the reservoir. The one is to set floating barriers downstream to prevent woody debris flow into the reservoir impounding area. The other method is to build a skimming wall to guide woody debris flow across the intake (Auel et al., 2011). However, setting a floating barrier is a commonly practiced method to trap woody debris in a reservoir; the extracted woody debris is placed in a nearby field (as shown in Fig. 1(b)(3) and 1(b)(4)).

The present study investigates the variation of the plunging region based on different hydraulic conditions and the suitable location of the floating barrier setup. Therefore, this study adopts the densimetric Froude number, plunging formula (modified from Parker and Toniolo, 2007), field observation, and associated estimation by experimental formula and parameters (Parker et al., 1987) in a reservoir. This study establishes a preliminary connection between turbidity current and woody debris. Additionally, the applicability of the regressed formulas to estimate the volume of woody debris was discussed. There are variations in flood discharge, grain size, and sediment concentration throughout a flood. Consequently, turbidity currents are unsteady concerning the inflow discharge, grain size distribution, sediment concentration, velocity, and thickness (Morris and Fan, 2010).

2. Study site description

The Shihmen Reservoir is a multi-purpose reservoir, and its functions include irrigation, domestic water supply, hydropower generation, flood prevention, and recreation. The irrigation area covered includes Taoyuan, Hsinchu, and Taipei, a total of 3.65 $\times 10^8$ m^2, implying its significance in agriculture. In addition, the reservoir serves 28 districts and 3.4 million people. Hence Shihmen Reservoir plays a vital role as a significant water resource contributor to the livelihood in northern Taiwan. The Shihmen Power Plant generates 2.3 $\times 10^8$ kWh (kilowatt per hour) annually utilizing the water impoundment at Shihmen Dam, offering a significant contribution to supplying peak demand for electricity and industrial development. Another function of the reservoir is to mitigate flood damage in the downstream areas during typhoons and heavy seasonal rains by reducing flood peak discharge.

The Shihmen Reservoir has a natural drainage area of 762.4 km^2 formed by the Shihmen Dam located upstream of the Dahan River and flowing westward to the Taiwan Strait. The Shihmen Dam, completed in 1963, is a 133 m high embankment dam with six spillways, one bottom outlet, two power plant intakes, one irrigation intake, and two tunnel spillways. The elevations above the sea level of the spillway crest, bottom outlet, power plant intake, irrigation intake, and tunnel spillway are EL.235 m, EL.169.5 m, EL.173 m, EL.192.5 m, and EL.220 m, respectively. The design capacity of the six spillways, one bottom outlet, power plant intakes, one irrigation intake, and two tunnel spillways are 11,400 m^3/s, 34 m^3/s, 137.2 m^3/s, 18.4 m^3/s, and 2400 m^3/s, respectively. With an average water level of EL.245 m, the reservoir impounding area covers a length of 16.5 km, and the water surface area of 8.15 km^2. The initial total storage capacity was 3.09 $\times 10^8$ m^3, and the active storage was 2.04 $\times 10^8$ m^3. Since the dam was completed, incoming sediment has settled rapidly along the reservoir bed due to a lack of desilting activities. As a result, according to the field survey, the longitudinal bed profile along the reservoir thalweg has accumulated significant deposits since the earliest dam operation. Since 2000, the depositional pattern has taken on a wedge-like appearance. Consequently, based on the recent survey data in 2022, the storage capacity was estimated to be 66.02 % of its initial capacity. The sediment deposition was classified as silt or clay based on particle size distribution sampled from outflow discharge (Huang et al., 2013).

Due to severe sediment deposition and woody debris problem during Typhoon Aere in 2004 (Fig. 2(a)), the stratified withdrawal facility was built beside the dam site in 2009 to ensure water supply capacity. In addition, one of the penstocks of the power plant was modified in 2012 for turbidity current venting. The stratified withdrawal work with three elevations (EL.220 m, EL.228 m, and EL.236 m) was completed in Dec. 2009. In addition, to protect power plant facilities from being damaged by woody debris moving with turbidity current, two floating barriers were installed at 9.0 km (Section 24) and 11.9 km (Section 27) away from the dam. Fig. 2 (b) and (c) show woody debris accumulation in the field at Section 24 during Typhoon Soudelor in 2015, and Typhoon Megi in 2016, respectively.

3. Hydrological conditions

Based on the field measurement, the suspended sediment concentration could be related to the inflow discharge, as shown in the following regression formula.

$$Q_s = aQ^m = 0.4546Q^{2.0544} \tag{1}$$

where a and m are the coefficients of the regression relationship; Q_s is inflow sediment discharge (ton/day);Q is inflow discharge (m^3/s). The regression data between discharge and sediment concentration from 1963 to 2022 of the Lofu station and the regression formula during typhoon floods are shown in Fig. 3. For many rivers, the rating exponent m was typically between 0.5 and 1.5 (Mulder and Syvitsky, 1995), and if m was determined from daily averaged or instantaneous measurements, its value could frequently reach 2.0. Therefore, the regression formula was usually reasonable to estimate the inflow sediment concentration. In addition, a sequence of measured data was collected at Lofu station during Typhoon Jangmi, as shown in Fig. 3. The measured data showed different regression formulas. When inflow discharge increased, the inflow sediment reached the maximum concentration before the peak inflow discharge. This phenomenon was similar to most mountainous regions and was discussed by Hager (1985) and De Cesare et al. (2001). The reaching time ratio of peak concentration to peak discharge was 0.67. The regression formula and measured data were used to estimate the location of the plunge point, and the comparison of the results will be discussed in this study.

4. Plunge point analysis

The plunge phenomenon can be defined as the transitional flow from homogeneous open channel flow to the stratified sediment-

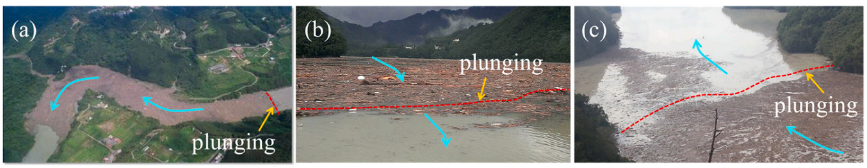

Fig. 2. Field observation of woody debris in the Shihmen Reservoir at (a) 13.6 km from the dam during Typhoon Aere in 2004, (b) 9 km from the dam during Typhoon Soudelor in 2015, and (c) 10 km from the dam during Typhoon Megi in 2016.

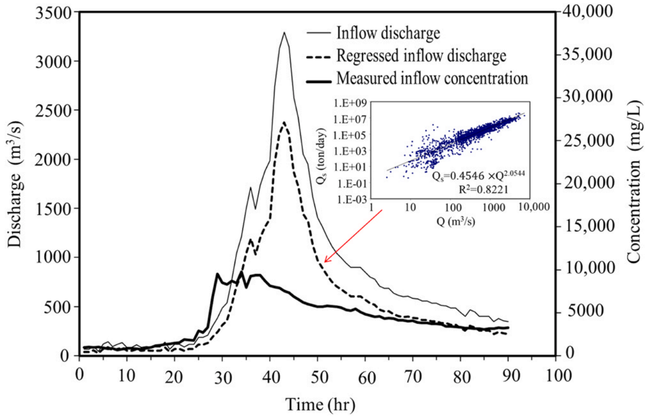

Fig. 3. Modeled inflow discharge and regressed inflow concentration at Lofu station in the flood event during Typhoon Jangmi.

laden flow (Akiyama and Stefan, 1984). In general, the flow field can be divided into four distinct regions: open channel, plunge area, turbidity current body, and head region, as shown in Fig. 1(a). As shown in Fig. 1(a), U_p is the depth-averaged velocity (m/s); H_p is the plunge depth (m); ρ_d is the layer-averaged density of turbidity current (kg/m^3); U_d is the layer-averaged velocity of turbidity current (m/s); H_d is the layer-averaged thickness of turbidity current (m); U_f is the head velocity of turbidity current (m/s); ρ_a is the density of ambient water (kg/m^3); U_a is the velocity of ambient water (m/s); H_a is the thickness of the ambient fluid (m).

Several plunge point experiments and numerical simulations have been studied and discussed in the introduction section. However, only a few studies had previously studied the movement relationship between woody debris and turbidity current. Most studies focused on the changes in the plunge point or vertical pattern distribution when the flow reached a steady state. The densimetric Froude number has been proposed to express the plunging condition as follows (Morris and Fan, 2010):

$$\frac{U_p}{\sqrt{\frac{\Delta\rho}{\rho_a} g H_p}} = F_r \tag{2}$$

where $\Delta\rho = \rho_d - \rho_a$; g= gravitational acceleration (m/s^2); F_r = densimetric Froude number, which experimentally ranges from 0.3 to 1.0 as mentioned in the introduction section. In addition, the theoretical condition of the plunging point location was developed and discussed by Akiyama and Stefan (1984) and Parker and Toniolo (2007). The densimetric Froude number was found equal to 1, just downstream of plunging on steep and mild bottom slopes. The plunging formula is expressed as follows:

$$\theta = \phi \times \left\{ \frac{1}{2(1+\lambda)} \left[\left(\frac{2+\lambda}{2} + 1 \right) + \sqrt{\left(\frac{2+\lambda}{2} + 1 \right)^2 - \frac{4}{1+\lambda}} \right] \right\} - 1 \tag{3}$$

where $\phi = \frac{H_d}{H_p}$, $\lambda = \frac{U_a(H_p - H_d)}{U_p H_p}$

Where θ is the critical value at the plunge point location, the critical value θ is approaching 0. Therefore, the plunging formula Eq. (3) can be used to estimate the plunge point location. Due to the mathematical limitation, Eq. (3) is not applicable when the value λ is less than 0. Besides, Eq. (3) can be used to assess the plunge point location and woody debris distribution during the typhoon flood event, and the entrainment formula (Eq. (4)) can be used to validate the plunge point location and plunge depth. The entrainment formula can be analyzed and expressed as follows (Parker et al., 1987; Graf and Altinakar, 1998):

$$\frac{d}{dx}(U_d H_d) = E_w U_d,\ E_w = \frac{0.075}{\sqrt{1 + 718 R_i^{2.4}}},\ R_i = \frac{1}{F_r^2} \tag{4}$$

where $E_w$is the entrainment parameter, and R_i is the Richardson number. The depth-averaged velocity (U_d) and the layer-averaged thickness (H_d) of the turbidity current are mentioned in Eq. (3) and (4) can be obtained from the measured data by adopting the following equations (Parker et al. 1987; Hosseini et al. 2006):

$$\begin{cases} U_d H_d = \int_0^\infty u_d(z) dz = \int_0^{H_t} u_d(z) dz \\ {U_d}^2 H_d = \int_0^\infty {u_d}^2(z) dz = \int_0^{H_t} {u_d}^2(z) dz \end{cases} \tag{5}$$

where H_t is the height at which $u_d(z)$ is zero.

5. Results and discussion

5.1. Turbidity current identification

Due to heavy rainfall, strong wind, and deep-water depth during the typhoon flood event, turbidity current is challenging to observe in the field. The event lasts briefly, particularly in Taiwan, making it difficult to observe a plunging phenomenon in time. The plunge location will move and depend on inflow hydrological conditions. Due to the color variation caused by the turbidity difference of sediment-laden flow, it is possible to identify the plunging point location using satellite images or closed-circuit television (CCTV) cameras. However, clouds usually cover the observation zone during heavy rainfall, making it rather difficult to determine the location of a plunge using imagery. Therefore, the vertical regression profile of turbidity current can aid in confirming the occurrence of a turbidity current. Hosseini et al. (2006) established two equations based on experimental data to describe the turbidity current vertical profiles of velocity and concentration distributions in Eqs. (6) and (7) respectively as follows:

$$\begin{cases} \dfrac{u_d(z)}{U_m} = \exp\left[-0.5\left(\dfrac{z}{H_m}-1\right)^{2.2}\right], z > H_m \\ \dfrac{u_d(z)}{U_m} = \left(\dfrac{z}{H_m}\right)^{0.33}, z \le H_m \end{cases} \tag{6}$$

$$\begin{cases} \dfrac{c_d(z)}{C_m} = \exp\left[-2.0\left(\dfrac{z}{H_m}-1\right)^{1.3}\right], \quad z > H_m \\ \dfrac{c_d(z)}{C_m} = \left(\dfrac{z}{H_m}\right)^{-0.7}, z \le H_m \end{cases} \tag{7}$$

where $u_d(z)$ is the velocity at distance z above the bed. $U_m$is the maximum velocity of turbidity current. $H_m$is the height of maximum velocity.$c_d(z)$ is the concentration at elevation z above the bed. $C_m$is the maximum concentration of turbidity current. Based on the analysis by Hosseini et al. (2006), three regions defined in the vertical profiles of the turbidity current include the inner region between the bed and velocity maximum, the outer region between the velocity maximum and zero velocity, and a shear–diffusion layer ($u_d(z)<$ 0) where the particles are affected by shear and diffusion.

During Typhoon Jangmi in 2008, the measured and sampled field data were collected by using the Portable Ultrasonic Device (PUD) (Huang et al., 2013) in the Shihmen Reservoir along the floating barrier line (located at, −25 m from the right side, the center and 25 m from the left side) positioned at cross Section 24 (9.0 km from the dam site). The inflow and outflow discharges through the reservoir were closely the same during the measurement period to retain the water surface elevation steady in the reservoir. Under such circumstances, the turbidity current could generate the vertical velocity profile consisting of a maximum velocity (U_m) within the body of the turbidity current. In the shear–diffusion layer ($u_d(z)<$ 0), the measured velocity with a negative value between the water surface and $u_d(z)=$ 0 indicates that there is backflow circulation in the ambient water above the turbidity current (See Fig. 4).

Therefore, the turbidity current generates a negative velocity gradient resulting from the backflow effect in the outer region, as shown in Fig. 4. The field-measured velocity data at various elevations showed a similar tendency of vertical velocity profile expressed in Eq. (6) by the solid line when $u_d(z)>$ 0. However, the trend is different while $u_d(z)$closed to zero in the outer region and$u_d(z)\le$ 0 in the shear–diffusion layer. The vertical velocity distribution when$z > H_m$ does not consider the circulation above the body of the turbidity current and suggests a suitable equation to describe it in Hosseini et al. (2006). Therefore, a new regressed equation when $z > H_m$is proposed to connect the outer region and shear–diffusion layer in Eq. (8). The proposed regressed equation of the vertical

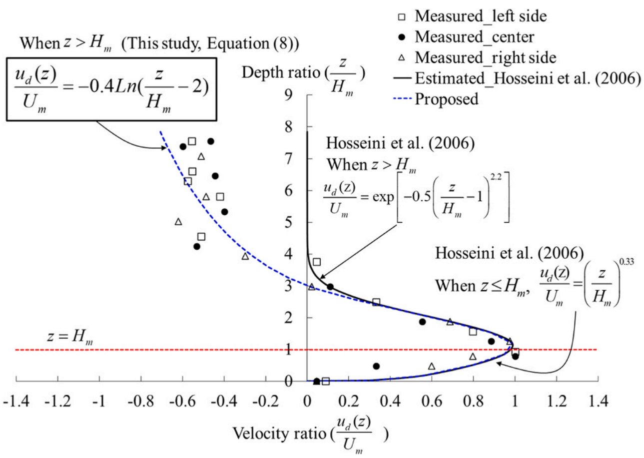

Fig. 4. Measured and estimated velocity at floating barrier downstream (9.0 km from the dam) in Shihmen Reservoir during Typhoon Jangmi.

profiles agreed with the measured results reported by Huang et al. (2013) when $z > H_m$. It reveals that the proposed regression equation can describe the vertical velocity profile of the shear-diffusion layer and improve the integrity of the entire vertical velocity profile between the water surface and the bed.

$$\frac{u_d(z)}{U_m} = -0.4Ln\left(\frac{z}{H_m} - 2\right), \quad z > H_m \tag{8}$$

For the vertical concentration profile, the field-measured data and the regression curve expressed by Eq. (7) are plotted in Fig. 5. However, field data does not fit well with the solid line, which may be attributed to sediment particle size or complex hydraulic factors. A proposed regression curve is shown by the dashed line (when $z > H_m$) in Fig. 5 and Eq. (9).

$$\frac{c_d(z)}{C_m} = \exp\left[-0.4\left(\frac{z}{H_m} - 1\right)^{1.3}\right], \quad z > H_m \tag{9}$$

Based on measured data collected at cross Section 24, this sampling location lies downstream of the plunge point. Therefore, Eqs. (2) and (3) can be used to calculate the plunge point location, and Eq. (4) can be used to validate the water depth at the plunge point location.

5.2. Variation of plunge point location

Based on field observations of areas commonly gathering drifting woody debris after multiple flood events, floating barriers were installed in 2008 at section 24 (9.0 km from the dam) and section 27 (11.9 km from the dam) to prevent woody debris from drifting toward the dam (Water Resources Planning Branch, 2008). The theoretical presumption is that woody debris floats with sediment-laden inflow and accumulates around the plunge point location. However, to select an appropriate location for the floating barrier and prevent the drift of woody debris towards the dam, it is crucial to carefully assess the plunge point location of the turbidity current, as indicated by field observations (Morris and Fan, 2010). The accumulation of floating woody debris, typically observed just upstream of the plunge point location, serves as a visible indicator of plunging phenomena. To determine the plunge point location, Eq. (2) can be utilized to calculate the densimetric Froude number in relation to the inflow hydrological conditions. In Fig. 3, hydrographs depicting inflow concentration are presented, showing data obtained through a regression formula and measured data. Generally, data on inflow concentration from the regression formula are more readily accessible than those obtained through field measurements.

To ensure reliability, continuous field measurement data during a flood event is considered more trustworthy than data obtained through a regression formula. The calculation of the densimetric Froude number (F_r) at each cross-section involves employing Eq. (2) with input data comprising hourly inflow discharge, suspended sediment concentration, and water depth prior to the plunge point location. The estimation of the specific gravity of the turbidity current relies on measured or regressed data of the inflow suspended sediment concentration. Additionally, a comparison can be facilitated by evaluating theoretical data, including average velocity and water depth at the plunge point location, based on cross-section and water level.

According to previous studies, as mentioned in the paragraph of the introduction, both flume tests and field measurements have indicated that the plunging point location occurs when the densimetric Froude number (F_r) falls within the range of 0.3–1. For the flood event during Typhoon Jangmi, densimetric Froude numbers between 0.3 and 1 were calculated at each cross-section along the distance away from the dam, as illustrated in Fig. 6. Fig. 6(a) presents the variation in spatial plunging point locations over time, using regression data in Eq. (1) and different F_r setting values (i.e., 0.3 or 1) in the time series of the flood hydrograph (refer to Fig. 3). The

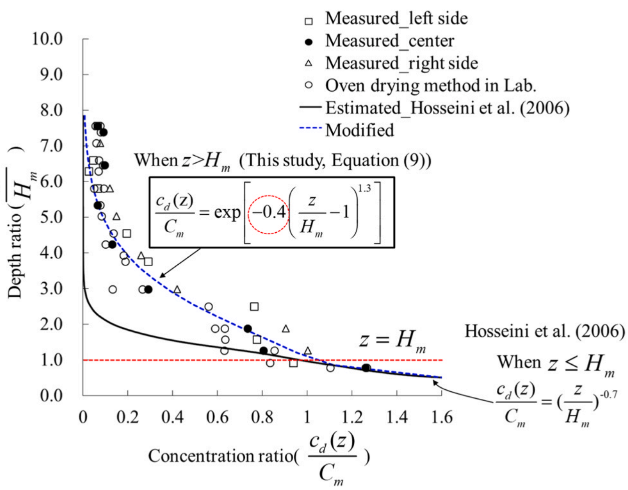

Fig. 5. Oven-dried, measured, and estimated sediment concentration at the floating barrier downstream (9.0 km from the dam) in Shihmen Reservoir during Typhoon Jangmi.

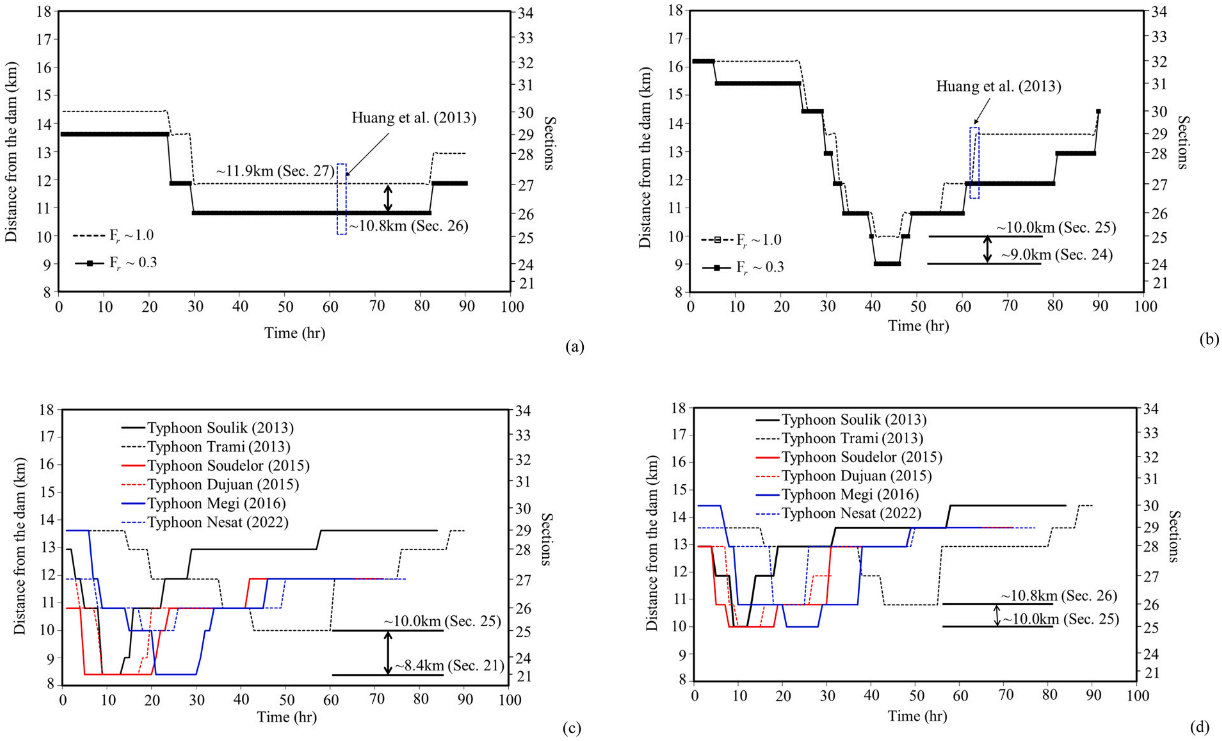

Fig. 6. Plunge point variation during (a) Typhoon Jangmi using regressed formula, (b) Typhoon Jangmi using measured data of Lofu station, (c) lower boundary of typhoon events between 2013 and 2022 using measured data of Lofu station, and (d) higher boundary of typhoon events between 2013 and 2022 using measured data of Lofu station.

interpretation of the densimetric Froude number varies with inflow discharge and concentration conditions, as demonstrated. Initially, during the onset of the flood event in Typhoon Jangmi, the plunge point location was situated between 13.6 km (section 29) and 14.4 km (section 30) away from the dam. However, as the inflow discharge increased and sediment concentration rose, the plunge point location migrated downstream. As the peak inflow discharge approached, the plunge point location was pushed further downstream, relocating between 10.8 km (section 26) and 11.9 km (section 27). During the recession period after 82 hours, the plunge point shifted backward in the upstream direction, settling between 11.9 km (section 27) and 12.9 km (section 28).

Fig. 6(b) illustrates the variation in densimetric Froude number during Typhoon Jangmi by incorporating the measured data of inflow suspended sediment concentration. This depiction further highlights the changing interpretation of the densimetric Froude number in response to varying inflow conditions. During the initial stages of Typhoon Jangmi, the plunge point location was situated more upstream than 16.2 km (section 32). However, as the inflow peak discharge approached, the plunge point shifted downstream, relocating between 9.0 km (section 24) and 10.0 km (section 25). In the recession period after 82 hours, the plunge point shifted backward in the upstream direction, settling between 12.9 km (section 28) and 14.4 km (section 30).

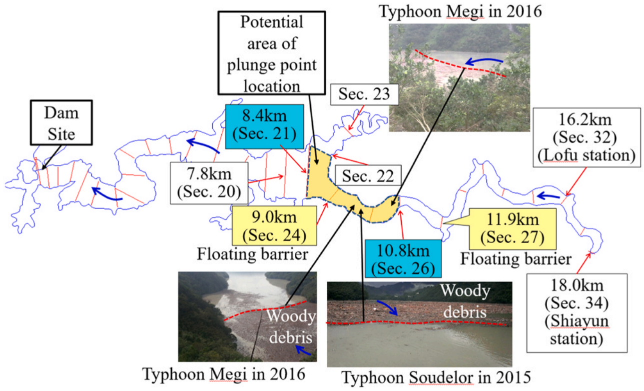

Fig. 7. Potential area of plunge point and woody debris collection during peak inflow discharge of typhoon events.

The potential sites of the plunge point location differ around peak inflow discharge, according to the results of various inflow concentration hydrographs. Utilizing data collected from typhoon events between 2013 and 2022, including measured inflow concentration at Lofu station, Figs. 6(c) and 6(d) provide an estimation of the potential area of the plunge point location during inflow peak discharge. The analysis reveals that the possible location of the plunge point location occurs between 8.4 km (section 21) and 10.8 km (section 26) during peak inflow discharge, as depicted in Fig. 7. This information proves valuable for the installation of the floating barrier, particularly in determining the lower boundary location of the woody debris collection area, especially during the recession period. Field observation of the woody debris collection area after typhoon events is presented in Fig. 7. The observed woody debris collection area ranged between 9.0 km (section 24) and 10.8 km (section 26). Concurrently, during the time of the photographs, the densimetric Froude number at 10.8 km (section 26) for Typhoon Soudelor and Typhoon Megi was recorded as 0.41 and 0.70, respectively.

For theoretical estimation, Eq. (3) was applied to calculate the plunge point location. However, the values of θ from 14.4 km (section 30) to 16.2 km (section 32) are deemed unreasonable due to the mathematical limitations of Eq. (3). Fig. 8 illustrates that the possible plunge point location is 12.9 km (section 28) during the measured duration. This result affirms that the measured data of inflow sediment concentration at Lofu station provides a more precise estimate of the plunge point location.

Additional evidence should be validated using the entrainment coefficient mentioned in Eq. (4). If the plunge point location is assumed to be at 12.9 km (section 28) during the measured duration at the floating barrier (9.0 km from the dam), the thickness of the turbidity current can be estimated. Fig. 9 illustrates the estimation results and compares them to the measured data at 9.0 km (section 24). The difference in turbidity current thickness aligns with both the measured data and estimated results. Based on the comparison results, the theoretical estimation agrees when the densimetric Froude number is close to 1.0, a value near the location of 12.9 km (section 28) during the measured duration.

5.3. Volume estimation of woody debris

Woody debris acts as a structural element of river systems by providing habitats for aquatic ecosystems in the mountain area. However, flood-induced turbid inflow discharge often carries woody debris from the upstream watershed due to steep slopes and high rainfall intensity. Usually, the Shihmen Reservoir might trap all the woody debris delivered to it during the flood events, which were then mechanically extracted from the reservoir. In the case of Typhoon Aere flood event in 2004, incoming heavy sediment-laden flow brought a great amount of woody debris with high sediment concentration into Shihmen Reservoir. As a result, massive woody debris was carried into the reservoir and damaged hydroelectric power facilities (see Fig. 1(b)). Typhoon Aere was analyzed close to the 100-year return-period flood of 8600 m^3/s. The extraction volume was about 54×10^3 m^3. In addition, the sediment concentration of the water-supply intake at Shihmen Reservoir in Typhoon Aere surpassed water treatment capability, reaching 179.8 $\times10^6$ (ton/day) (Tan et al., 2011). Consequently, the Taoyuan area experienced an 18-day water deficit due to the high silt content. In the following year 2005, Typhoon Matsa traversed Taiwan and resulted in 20 $\times10^3$ m^3 total extraction volume of woody debris (Water Resources Planning Branch, 2008). More data have been collected in flood events and listed in Table 1. By referring to woody debris quantity surveyed on the upper Rhone River (France), Moulin and Piegay (2004) estimated woody debris volume extracted from the Genissiat dam's reservoir by using a linear regression formula related to the peak flow discharge.

According to field surveys of the flood events, most of the extracted woody debris pieces investigated were classified as coniferous wood and broadleaf wood, which included the coniferous class: Chamaecyparis formosensis, Calocedrus formosana, Cunninghamia lanceolata and Cryptomeria japonica, and the broadleaf class: Cyclobalanopsis gilva, Cinnamomum camphora, Michelia formosana, and Alnus formosana (Water Resources Planning Branch, 2008). Due to various hydrological and morphological characteristics, the

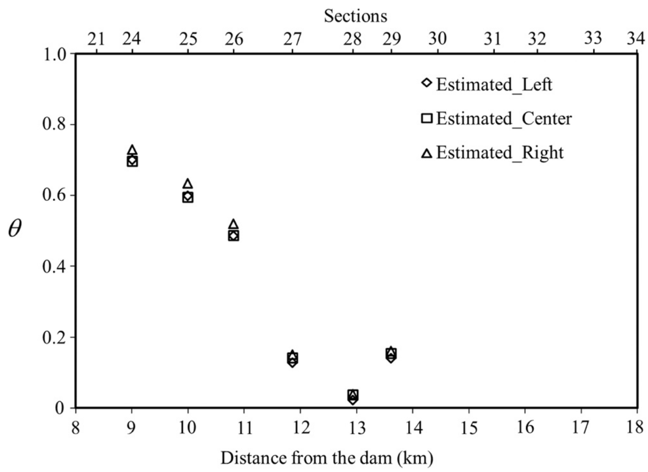

Fig. 8. Plunge point location assessment using the plunging formula (Eq. (3)) (Modified from Parker and Toniolo, 2007) in the Shihmen Reservoir during Typhoon Jangmi.

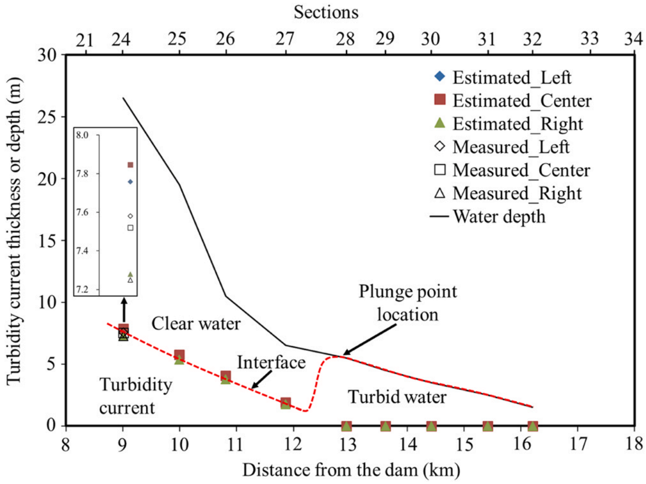

Fig. 9. Turbidity current thickness assessment based on entrainment estimation in the Shihmen Reservoir during Typhoon Jangmi.

Table 1
Events and hydrological values for the volume estimation of woody debris.

Typhoon Events	Date (yy/mm/dd)	Q_p (m^3/s)	Q_{sp} (10^3 ton/day)	ΣQ_s (10^3 ton)	R_{ip} (mm/hr)	ΣR_i (mm)	Measured W_v (10^3 m^3)
Aere	2004/08/23	8594	54959.19*	30045.83*	48.60	974.00	54.00
Matsa	2005/08/03	5322	20534.19*	5167.50*	42.90	860.40	20.00
Krosa	2007/10/04	5300	20360.19*	9751.68*	42.10	666.40	10.23
Jangmi	2008/09/26	3292	7966.71	4086.00	30.70	427.10	5.08
Morakot	2009/08/05	1838	2591.00	1840.00	17.40	471.30	1.62
Fanapi	2010/09/17	1056	169.00	201.00	23.00	166.60	3.96
Saola	2012/07/30	5385	15473.00	7651.00	44.30	830.80	9.10
Soulic	2013/07/11	5458	38396.00	9219.00	94.20	450.00	25.31
Trami	2013/08/20	2412	9813.00	3205.00	29.60	525.30	4.25
Soudelor	2015/08/06	5634	8902.00	2542.00	52.70	500.80	7.01
Dujuan	2015/09/27	3802	5204.00	1882.30	39.40	334.40	2.32
Megi	2016/09/25	4268	8562.00	3510.00	46.20	442.00	10.02
Nesat	2022/10/15	1750	1533.41	672.00	26.70	308.60	4.21

* Estimated using Eq. (1)

linear regression formula may be adjusted to estimate the historical extracted volume data in Shihmen Reservoir. However, the linear regression formula was not appropriate to estimate the annual-based woody debris extracted volume. The annual extracted woody debris might decrease over time. For instance, the annual extraction volume of woody debris from 2007 to 2008 was approximately 10, 227 m^3 and 5077 m^3, respectively.

Based on the data obtained from the Northern Region Water Resources Office (2020), the extraction volume of woody debris (W_v) in each flood event was measured from 2004 to 2022 to establish the relationships that may be related to inflow peak discharge (Q_p) or inflow peak sediment yield (Q_s), as shown in Figs. 10(a) and (b), respectively. In Fig. 10(a), the maximum value of inflow peak discharge of 8600 m^3/s occurred in 2004 Typhoon Aere with the extracted woody debris of 54×10^3 m^3. The relationship by linear regression (with R^2=0.65) agrees well between the inflow peak discharge and the extraction volume of woody debris in these thirteen flood events as listed in Table 1. Additionally, adopting the regressed relationship, the volumes of floating woody debris from the upstream watershed for various return-period flood discharges can be estimated to count the cost of the extraction operation. As presented in Fig. 10(a), the regressed line extends and has an intersection with the inflow peak discharge axis, which may illustrate there is a threshold value of the inflow peak discharge to initiate the occurrence of floating woody debris entering the reservoir. The inflow discharge threshold is about 1994 m^3/s to bring floating woody debris from the upstream watershed into the reservoir, which can be a warning index for the preparedness of the woody debris extraction operation.

Moreover, the extracted woody debris in each flood event may be related to the inflow sediment yield, aiding in estimating the amount of woody debris entering the Shihmen Reservoir. In Fig. 10(b), the inflow peak sediment yield (Q_{sp}) of 54959.19×10^3 ton/day in 2004 Typhoon Aere flood with the extracted woody debris of 54×10^3 m^3. The linear regression relationship (with R^2=0.91) fits well between the inflow peak sediment yield and the extraction volume in these thirteen events. From field observation in the reservoir, the sediment-laden inflow may carry more woody debris while the inflow sediment yield is high. In addition, in order to make this regression relationship more general and be applied in other contexts,ΣQ_p (represents the quantitative volume of peak inflow) is adapted to create a dimensionless regression line of inflow peak sediment yield.

On the other hand, the total inflow sediment yield (ΣQ_s) is directly linked to the volume of woody debris, as depicted in Fig. 10(c). A

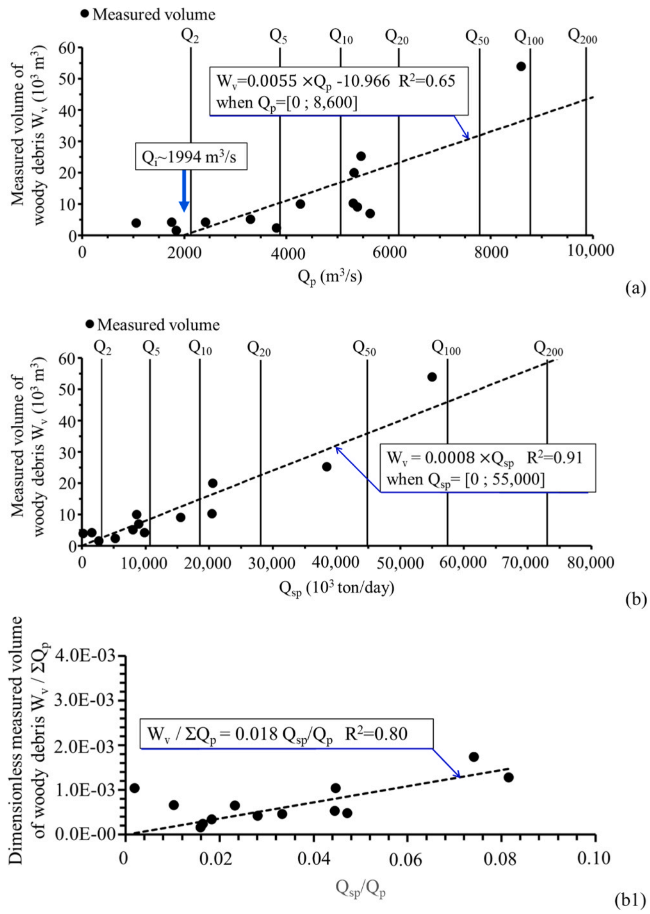

Fig. 10. The relationship between the measured extraction volume of woody debris and (a) inflow peak discharge (m^3/s), (b) inflow peak sediment yield (ton/day), (b1) dimensionless inflow peak sediment yield (ton/day), (c) total inflow sediment yield (ton), (d) maximum rainfall intensity (mm/hr), (e) total rainfall (mm).

higher induced inflow sediment yield may signify an increased capacity for woody debris generation. Nevertheless, the correlation coefficient (R^2) does not adequately capture the relationship compared to the peak inflow discharge and total inflow sediment yield. This suggests that the instantaneous intensity of the hydrological pattern of inflow peak sediment yield holds greater significance for woody debris production.

There are ten rain gauge stations in the Shihmen Reservoir catchment. Since the spatial distribution of rain gauge stations in the catchment area is not uniform, the Thiessen polygons method is employed to determine the influence control area of each rainfall station and obtain the Thiessen polygons weighting factor of each rain gauge station. In order to calculate the rainfall intensity and total rainfall in each flood event, the hourly historical rainfall records at each station were collected and multiplied by the Thiessen polygons weighting factor at each station to obtain the average rainfall of the watershed. Hereby, the maximum rainfall intensity (R_{ip}) and total rainfall (ΣR_i) are also related to the extracted woody debris by regression, as shown in Figs. 10(d) and 10(e), respectively. Regression results reveal that the regression relationship of total rainfall (Fig. 10(e)) is not better than that of maximum rainfall intensity (Fig. 10(d)), and this result is similar to Figs. 10(b) and 10(c). Practically, if the rainfall forecasting data is available from the precipitation models, the volume of woody debris entering the reservoir may be calculated for the decision maker to prepare woody debris extraction operation.

6. Conclusions

The feasibility of determining the plunge point location using field observation data and three methods, which include the densimetric Froude number, plunging formula, and entrainment formula, is investigated and analyzed. Therefore, the measured vertical velocity and sediment concentration of a turbidity current, the plunging formula and the entrainment formula in Typhoon Jangmi were used to investigate the plunge point location. Two proposed and modified equations are also provided to identify turbidity current vertical profiles of velocity and sediment concentration in Figs. 4 and 5. Although the plunging formula was limited to a

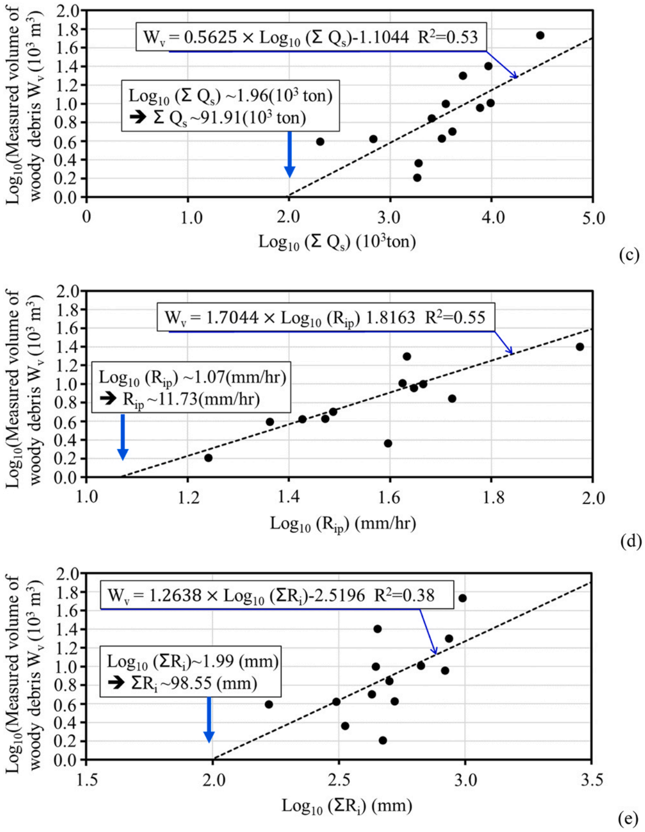

Fig. 10. (*continued*).

distinct area, it was suitable for most calculation ranges even though the thickness of the turbidity current was higher than the plunge depth. The entrainment mechanism dominated the thickness development of turbidity current along with the flow distance. Therefore, the thickness estimation of the plunge point location was assessed using measured data at the floating barrier (at Section 24, 9.0 km from the dam site). The inflow sediment concentration is generally estimated from the regression formula established at the hydrological station utilizing the relationship between discharge and suspended sediment. However, the regression formula typically does not depict the field sediment concentration hydrograph accurately. Therefore, this study adopts the measured data and the regression formula of sediment concentration to estimate the plunge point location and discuss the location difference.

Based on the flow mechanism at the plunge point location, woody debris could be collected near the plunge point location during flood events. Regarding the strength of the floating structure design and the prevention of woody debris flowing toward the dam after flood events, the downstream bound or next downstream section of the plunge point location is relatively feasible for floating barrier establishment. Therefore, for establishing the floating barrier near or slightly downstream of the plunge point location, the critical condition of densimetric Froude number (F_r=1.0) is suggested to estimate the plunge point location in this research. Implying 8.4 km (section 21) or 7.8 km (section 20) are suitable locations to set up the prevention structures for woody debris in the Shihmen Reservoir.

Based on the thickness validation of plunging depth using the entrainment mechanism at the measured location, the plunging point depth possessed a similar thickness value between the entrainment formula (Eq. (4)) and the plunging formula (Eq. (3)). The meanings of these results pointed out that the entrainment mechanism was not affected by the reservoir shape between sections. Therefore, the entrainment formula (Eq. (4)) and the plunging formula (Eq. (3)) can be assumed to predict a possible plunge point estimation.

In addition, this study presents five empirical relationships for the extraction volume estimation of woody debris. The study investigates the relationship between woody debris extraction and various hydrological parameters during flood events in the Shihmen Reservoir catchment. The analysis reveals a significant correlation between the inflow peak discharge and the extraction volume of woody debris, with a threshold inflow discharge of approximately 1994 m^3/s identified as the discharge in which woody debris begins to enter the reservoir. The threshold phenomenon is also present in rainfall patterns. This threshold serves as a critical warning indicator for the preparation of extraction operations. Additionally, a strong relationship is observed between the inflow peak sediment yield and the volume of extracted woody debris, indicating that higher sediment yields tend to carry more woody debris into the reservoir. Despite the total inflow sediment yield showing some correlation with woody debris volume, the inflow peak sediment yield is more indicative of woody debris production. The study also assesses the impact of rainfall intensity and total rainfall on woody debris extraction, finding that maximum rainfall intensity has a better correlation with the volume of woody debris than total rainfall. This suggests that peak-intensity events are more crucial for predicting the amount of the extracted woody debris.

7. Summary

The present study proposed two equations (Eq. (8) and Eq. (9)) to identify the turbidity current vertical profile. Then the user can attempt to define the plunging zone of turbidity current in correlation with the floating woody debris using field observations and presented formulas which includes Eq. (2), Eq. (3) and Eq. (4). It can help with the design of the floating barrier. In addition, this study presents five empirical relationships for the extraction volume estimation of woody debris. Considering hydrological conditions, the inflow peak sediment yield has an optimal relationship to estimate woody debris volumes than inflow peak discharge, total inflow sediment yield, maximum rainfall intensity, and total rainfall. The presented threshold values for the preparation of extraction operations for floating woody debris in Figs. 10(a), (c), (d) and (e) of hydrological patterns serve as a critical warning indicator.

The previous studies in the literature were limited to discussing the volume estimation of woody debris related to flood peak discharge. However, our study is the pioneer investigator on the relationship between varied hydrological patterns and the volume of woody debris. It reveals that our results and presented data are beneficial to woody debris estimation issues and help for future advanced studies. The relationship R^2 between the measured extraction volume of woody debris and adapted variables may consider dimensionless terms of normalization to improve quality and make results more generalizable and applicable to others in the future.

Ethics

Not applicable.

Funding

The financial support for this study was provided by a grant from the National Science and Technology Council.

Consent to Participate

Not applicable.

Consent to Publish

Not applicable.

CRediT authorship contribution statement

Tetsuya Sumi: Supervision, Resources. **Jihn-Sung Lai:** Writing – review & editing, Validation, Data curation. **Fong-Zuo Lee:** Writing – original draft, Methodology, Investigation. **Sameh Ahmed Kantoush:** Methodology, Formal analysis, Conceptualization.

Declaration of Competing Interest

The authors declare the following financial interests/personal relationships which may be considered as potential competing interests: Fong-Zuo Lee reports financial support was provided by National Science and Technology Council. Not applicable. reports a relationship with Not applicable. that includes:. Not applicable. has patent Not applicable. pending to Not applicable. Not applicable. If there are other authors, they declare that they have no known competing financial interests or personal relationships that could have appeared to influence the work reported in this paper

Acknowledgments

The presented study was supported by the National Science and Technology Council in Taiwan, and its Project number are NSTC 111–2221-E-005–092, NSTC 113-2625-M-002-018 and NSTC 113-2221-E-005-027. The writers wish to thank the Water Resources Agency, Hydrotech Research Institute National Taiwan University, and Disaster Prevention Research Institute of Kyoto University in Japan for their data, human resources, and technique support.

Data availability

Data will be made available on request.

References

Akiyama, J., Stefan, H.G., 1984. Plunging flow into a reservoir: theory. J. Hydraul. Eng. 110 (4), 484–499. https://doi.org/10.1061/(ASCE)0733-9429(1984)110:4(484).

Auel, C., et al., 2011. Design and construction of the sediment bypass tunnel at Solis. Int. J. Hydropower Dams 18 (3), 62–66.

Bournet, P., et al., 1999. Numerical investigation of plunging density current. J. Hydraul. Eng. 125 (6), 584–594. https://doi.org/10.1061/(ASCE)0733-9429(1999)125:6(584).

Brasington, J., Richards, K., 2000. Turbidity and suspended sediment dynamics in small catchments in the Nepal Middle Hills. Hydrol. Process. 14 (14), 2559–2574. https://doi.org/10.1002/1099-1085(20001015)14:14<2559::AID-HYP114>3.0.CO;2-E.

Busico, G., Kazakis, N., Cuoco, E., Colombani, N., Tedesco, D., Voudouris, K., Mastrocicco, M., 2020. A novel hybrid method of specific vulnerability to anthropogenic pollution using multivariate statistical and regression analyses. Water Res. 171, 115386.

Chang, M.J., et al., 2020. Development of a real-time forecasting model for turbidity current arrival time to improve reservoir desilting operation. Hydrol. Sci. J. 65 (6), 1022–1035. https://doi.org/10.1080/02626667.2020.1714628.

Chen, P.A., 2017. Reservoir turbidity-current arrival time and venting efficiency forecasting using machine learning. National Taiwan University.

Chen, P.A., 2022. Integration of multiple outlets' operation and sediment management options in the reservoir for increasing efficiency of turbidity current venting and clear water storages. Kyoto University.

Crimaldi, M., Lama, G.F.C., 2021. Impacts of riparian plants biomass assessed by UAV-acquired multispectral images on the hydrodynamics of vegetated streams, 2021 29th Eur. Biomass-.-. Conf. Exhib. 1157–1161. https://doi.org/10.5071/29thEUBCE2021-4AV.3.6.

Dai, A., Garcia, M.H., 2007. Discussion of "Note on the Analysis of Plunging of Density Flows" by Gary Parker and Horacio Toniolo. J. Hydraul. Eng. 135 (6), 690–694. https://doi.org/10.1061/(ASCE)HY.1943-7900.0000005.

Dai, A., Garcia, M.H., 2009a. Analysis of plunging phenomena. J. Hydraul. Res. 47 (5), 638–642. https://doi.org/10.3826/jhr.2009.3498.

Dai, A., Garcia, M.H., 2009b. Discussion of Plunging condition of two-dimensional negative buoyant surface jets released on a sloping bottom. J. Hydraul. Res. 47 (5), 681–682. https://doi.org/10.1080/jhr.2008.2714a.

De Cesare, G., et al., 2001. Impact of turbidity current on reservoir sedimentation. J. Hydraul. Eng. 127 (1), 6–16. https://doi.org/10.1061/(ASCE)0733-9429(2001)127:1(6).

Ehmann, K., et al., 2019. Monitoring turbidity from above: deploying small unoccupied aerial vehicles to image in-stream turbidity. Hydrol. Process. 33 (6), 1013–1021. https://doi.org/10.1002/hyp.13372.

Ettema, R., Arndt, R., Robert, P., Wahl, T., 2000. Hydraulic modeling - concepts and practice. ASCE publications, Reston, VA.

Farrel, G.J., Stefan, H., 1988. Mathematical modeling of plunging reservoir flows. J. Hydraul. Res. 26 (5), 525–537. https://doi.org/10.1080/00221688809499191.

Graf, W.H., 1983. The behaviour of silt-laden current. Int. Water Power dam Constr. 35 (9), 33–38.

Graf, W.H., Altinakar, M.S., 1998. Fluvial hydraulics: Flow and transport processes in channels of simple geometry. Wiley, New York.

Hager, W.H., 1985. A simplified hydrological rainfall-runoff model—Reply. J. Hydrol. 80 (3-4), 397–398. https://doi.org/10.1016/0022-1694(85)90132-5.

Hebbert, B., et al., 1979. Collie river underflow into the wellington reservoir. J. Hydraul. Div. 105 (5), 533–545. https://doi.org/10.1061/JYCEAJ.0005206.

Hosseini, S.A., et al., 2006. Synchronous measurements of the velocity and concentration in low density turbidity currents using an Acoustic Doppler Velocimeter. Flow. Meas. Instrum. 17 (1), 59–68. https://doi.org/10.1016/j.flowmeasinst.2005.05.002.

Huang, Y.J., et al., 2013. Measurements of solid suspension concentration and flow velocity with temperature compensation in one portable ultrasonic device. Hydrol. Sci. J. 58 (3), 615–626. https://doi.org/10.1080/02626667.2012.714469.

Huang, C.C., Ho, H.C., Lai, J.S., Lee, F.Z., 2023. Experimental study with hydraulic modeling of a reservoir desilting operation using a sediment bypass tunnel. Environ. Earth Sci. 82 (12), 313. https://doi.org/10.1007/s12665-023-10992-2.

Hung, C.C., et al., 2022. An efficient and economic desiltation strategy for reservoir sustainable development under the threat of extreme flooding threaten. J. Water Clim. Change 13 (3), 1257–1274. https://doi.org/10.2166/wcc.2022.353.

Hung, C.C., 2024. Navigating reservoir deposition challenges: evaluation of reservoir desilting strategy through a 4-stage life cycle assessment approach, 2024 Water Resour. Manag.. https://doi.org/10.1007/s11269-024-03847-3.

Imtiyaz, N., Lee, F.Z., Lin, G.F., Lai, J.S., 2024. Modeling and analysis of turbidity currents in a reservoir with the dredged guiding channel. KSCE J. Civ. Eng. 1–13.

Jain, S.C., 1981. Plunging phenomena in reservoirs. In Surface Water Impoundments. ASCE, pp. 1249–1257.

Lama, G.F.C., Rillo Migliorini Giovannini, M., Errico, A., Mirzaei, S., Chirico, G.B., Preti, F., 2021. The impacts of Nature Based Solutions (NBS) on vegetated flows' dynamics in urban areas. 2021 IEEE Int. Workshop Metrol. Agric. For. (MetroAgriFor) 2021, 58–63. https://doi.org/10.1109/MetroAgriFor52389.2021.9628438.

Lee, F.Z., et al., 2019. Turbidity current plunge mechanism analysis and simulation system application. Taiwan Water Conserv. 67 (4), 1–15.

Lee, F.Z., et al., 2022. Reservoir sediment management and downstream river impacts for sustainable water resources-case study of Shihmen Reservoir. Water 14 (3), 479. https://doi.org/10.3390/w14030479.

Lee, F.Z., Huynh Nguyen, N.L., 2024. Application of artificial countermeasures to enhance desilting efficiency in a reservoir under normal and extreme events. J. Water Clim. Change 15 (6), 2649.

Lee, H.Y., Yu, W.S., 1997. Experiment study of reservoir turbidity current. J. Hydraul. Eng. 123 (6), 520–528. https://doi.org/10.1061/(ASCE)0733-9429(1997)123:6(520).

Lense, G.H.E., Lämmle, L., Ayer, J.E.B., Lama, G.F.C., Rubira, F.G., Mincato, R.L., 2023. Modeling of soil loss by water erosion and its impacts on the cantareira system, Brazil. Water 15, 1490. https://doi.org/10.3390/w15081490.

Minella, J.P.G., et al., 2008. Estimating suspended sediment concentrations from turbidity measurements and the calibration problem. Hydrol. Process. 22 (12), 1819–1830. https://doi.org/10.1002/hyp.6763.

Morris, G.L., Fan, J., 2010. Reservoir sedimentation handbook. Electron. Version.

Moulin, B., Piegay, H., 2004. Characteristics and temporal variability of large woody debris trapped in a reservoir on the river RHONE: implications for river basin management. River Res. Appl. 20 (1), 79–97. https://doi.org/10.1002/rra.724.

Mulder, T., Syvitsky, J.P.M., 1995. Turbidity currents generated at river mouths during exceptional discharges to the world oceans. J. Geol. 103 (3), 285–299.

Northern Region Water Resources Office (2020). Sediment Transport Monitoring Facility Maintenance and Flood Event Observations in Shihmen Reservoir. Water Resources Agency, MOEA, Taiwan.

Panagos, P., et al., 2024. Understanding the cost of soil erosion: an assessment of the sediment removal costs from the reservoirs of the European Union. J. Clean. Prod. 434, 140183.

Parker, G., et al., 1987. Experiment on turbidity currents: theory and observation. J. Hydraul. Res. 25 (1), 123–147. https://doi.org/10.1080/00221688709499292.

Parker, G., Toniolo, H., 2007. Note on the analysis of plunging of density flows. J. Hydraul. Eng. 133 (6), 690–694. https://doi.org/10.1061/(ASCE)0733-9429(2007)133:6(690).

Pirone, D., Cimorelli, L., Pianese, D., 2024. The effect of flood-mitigation reservoir configuration on peak-discharge reduction during preliminary design. J. Hydrol.: Reg. Stud. 52, 101676. https://doi.org/10.1016/j.ejrh.2024.101676.

Ruiz-Villanueva, V., et al., 2013. Reconstruction of a flash flood with large wood transport and its influence on hazard patterns in an ungauged mountain basin. Hydrol. Process. 27 (24), 3424–3437. https://doi.org/10.1002/hyp.9433.

Savage, S.B., Brimberg, J., 1975. Analysis of plunging phenomena in water reservoirs. J. Hydraul. Resour. 13 (2), 187–205. https://doi.org/10.1080/00221687509499713.

Schleiss, A.J., et al., 2016. Reservoir sedimentation. J. Hydraul. Res. 54 (6), 595–614.

Seo, J.I., et al., 2012. Large wood export regulated by the pattern and intensity of precipitation along a latitudinal gradient in the Japanese archipelago. Water Resour. Res. 48 (3). https://doi.org/10.1029/2011WR010880.

Singh, B., Shah, C.R., 1971. Plunging phenomenon of density currents in reservoirs. Houille Blanc 26 (1), 59–64.

Tan, Y.C., et al., 2011. Complex disaster damaged to water resources in Taiwan. 21st Int. Congr. Irrig. Drain. 56.

Vaughn, T., et al., 2021. Floating woody debris: blocking sensitivity of Labyrinth weirs in channel and reservoir applications. J. Hydraul. Eng. 147 (11), 06021016. https://doi.org/10.1061/(ASCE)HY.1943-7900.0001937.

Wang, S., et al., 2013. Effects of different operational modes on the flood-induced turbidity current of a canyon-shaped reservoir: case study on Liuxihe Reservoir, South China. Hydrol. Process. 27 (26), 4004–4016. https://doi.org/10.1002/hyp.9534.

Water Resources Planning Branch, 2008. Driftwood motion and turbidity current in Shihmen Reservoir: experiments and analyses. Water Resources Agency, MOEA, Taiwan.

Water Resources Planning Branch, 2020. RESERVOIR DESILTATION: Technology and Management. Water Resources Agency, MOEA, Taiwan.

Wunderlich, W.O. and Elder, R.A., 1973. Mechanism of flow through man-made lakes, Man-made Lakes: their problems and environmental effects. C. Ackermann, G. F. White, and E. B. Worthington, eds., Am. Geophys. Union, Washington, D. C.